PCCP

PAPER

View Article Online
View Journal | View Issue

Cite this: *Phys. Chem. Chem. Phys.*, 2018, **20**, 26597

Influence of the metals and ligands in dinuclear complexes on phosphopeptide sequencing by electron-transfer dissociation tandem mass spectrometry†

Daiki Asakawa, *[a] Akio Miyazato,[b] Frédéric Rosu [c] and Valérie Gabelica [d]

Phosphorylation is one of the most important protein modifications, and electron-transfer dissociation tandem mass spectrometry (ETD-MS/MS) is a potentially useful method for the sequencing of phosphopeptides, including determination of the phosphorylation site. Notably, ETD-MS/MS typically provides useful information when the precursor contains more than three positive charges. It is not yet used as an analysis method for large-scale phosphopeptide production due to difficulties occurring in the production of acidic phosphopeptides having more than three positive charges. To increase the charge state of phosphopeptides, we used dinuclear metal complexes, which selectively bind to the phosphate group in phosphopeptides with the addition of positive charge(s). Dinuclear copper, zinc, and gallium complexes were tested and it was found that the type of metal present in the complex strongly affected the affinity of the phosphorylated compounds and their ETD fragmentation. The dinuclear copper complex interacted weakly with the phosphate groups and ETD-induced peptide fragmentation was largely suppressed by the presence of Cu^{2+}, which worked as an electron trap. The dinuclear gallium complex was strongly bound to a phosphate group. However, the ligand binding to gallium acted as an electron trap and the presence of dinuclear gallium complex in the precursor for ETD-MS/MS hampered the sequencing of the phosphopeptides, as in the case of dinuclear copper complexes. In contrast, dinuclear zinc complexes efficiently bind to phosphopeptides with an increase in the charge state, facilitating phosphopeptide sequencing by ETD-MS/MS. The fragmentation of the ligand and peptide backbone in the dinuclear zinc–phosphopeptide complex were competitively induced by ETD. These processes are influenced by the ligand structure and so the detailed ETD fragmentation pathways were investigated using density functional theory calculations.

Received 17th July 2018,
Accepted 22nd September 2018

DOI: 10.1039/c8cp04516j

rsc.li/pccp

Introduction

The reversible phosphorylation of proteins is a common covalent protein modification,[1,2] and electrospray ionization (ESI)-based tandem mass spectrometry (MS/MS) is currently the dominant method for the analysis of protein phosphorylation. In particular, collision-induced dissociation (CID) has been widely used to analyze the peptide sequence by MS/MS. In the CID of phosphorylated peptides, the loss of the phosphate groups (80 and 98 Da) can be used as a specific marker for phosphorylated peptide identification.[3,4] Therefore, the screening of phosphorylated peptides can be achieved by CID-MS/MS. However, the determination of the phosphorylated sites in peptides is hindered by the substantial loss of the phosphate groups because most of the fragment ions are observed in a non-phosphorylated form in CID-MS/MS spectra.[3,5,6]

Fragmentation methods involving the electron association of multiply charged peptides, such as electron-capture dissociation (ECD)[7] and electron-transfer dissociation (ETD),[8] have been used as alternative methods to CID.[9–11] Because the ECD/ETD of phosphorylated peptides results in fragment ions arising from the fragmentation of the peptide backbone without losing phosphoric acid, the determination of the phosphorylation site is possible. Regarding the ECD/ETD mechanism,

[a] *National Institute of Advanced Industrial Science and Technology (AIST), National Metrology Institute of Japan (NMIJ), Tsukuba Central 2, 1-1-1 Umezono, Tsukuba, Ibaraki, 305-8568, Japan. E-mail: d.asakawa@aist.go.jp; Tel: +81-029-861-0586*
[b] *Center for Nano Materials and Technology, Japan Advanced Institute of Science and Technology, 1-1 Asahidai, Nomi, Ishikawa, Japan*
[c] *CNRS, INSERM, Univ. Bordeaux, Institut Européen de Chimie et Biologie (IECB, UMS3033, US001), 2 rue Robert Escarpit, 33607 Pessac, France*
[d] *Univ. Bordeaux, INSERM, CNRS, Laboratoire Acides Nucléiques Régulations Naturelle et Artificielle (ARNA, U1212, UMR5320), IECB, 2 rue Robert Escarpit, 33607 Pessac, France*

† Electronic supplementary information (ESI) available. See DOI: 10.1039/c8cp04516j

electron attachment/transfer occurs competitively at positively charged sites[12] and at the π^* antibonding orbital of peptide bond[13–15] in multiply charged peptides, leading to N–Cα bond cleavage through aminoketyl radical intermediates. Although one of the most promising applications of ECD/ETD is phosphopeptide sequencing, it has not yet become the method of choice for large-scale phosphopeptide analysis because of the low fragmentation efficiency for tryptic phosphopeptides.[16]

Employing ions with a higher charge state as the precursors for ECD/ETD is a way to dramatically improve the fragmentation efficiency by increasing the yield of reactive radical species, which can thereby improve the sequence coverage.[17–19] Here, we investigated how to increase the charge state of precursor ions to improve the quality of ETD mass spectra. In particular, the complexation of peptides with metal ions has been demonstrated to increase the charge state of peptides and various metal cations have been used as the cationization adductive for ETD-MS/MS experiments.[20–24] With regards to the ETD processes, the metal–peptide complex undergoes either N–Cα bond cleavage or metal cation reduction, according to the electrochemical properties of the metal cations in the precursor. The metal cation having a closed shell, such as monovalent alkali metal cations, divalent alkali earth and group XII metal cations, and trivalent group XIII metal cations are barely reduced under ETD-MS/MS conditions.[25–28] In consequence, the use of a metal cation having a closed shell promotes the N–Cα bond cleavage and provides more informative MS/MS mass spectra compared to those obtained from protonated precursors with lower charge states.[21,22,29] In contrast, transition metal cations with a partially filled d orbital shell, such as Co^{2+}, Ni^{2+}, and Cu^{2+}, are reduced by ETD and the fragmentation is mainly induced by the substantial excitation attributable to the reduction energy of the metal cation in the complex.[30] Although Cd^{2+} and Hg^{2+} are closed shelled metal cations, Cd^{2+}– and Hg^{2+}–peptide complexes undergo metal cation reduction by ETD, probably due to complex electron energy levels of Cd^{2+} and Hg^{2+}.[22,31] The results suggest that the period 5, 6, and 7 metal cations were susceptible to undergoing reduction by ETD. Therefore, alkali metals, alkaline earth metals, Al^{3+}, Zn^{2+}, and Ga^{3+} are suggested to be suitable adductives for peptide sequencing by ETD-MS/MS. However, the yield of the metal–peptide complex is usually low when the free metal cation is used.[21,22,30]

To increase the yield of the metal–phosphopeptide complex, we recently used a dinuclear zinc complex, $(Zn_2L1)^{3+}$ (L1 = alkoxide form of 1,3-bis[bis(pyridin-2-ylmethyl)amino]propan-2-ol), also known as the phosphate-capture molecule ''phos-tag'',[32–34] as an ionizing reagent.[16] The molecular structure of $(Zn_2L1)^{3+}$ is shown in Scheme 1a. Because $(Zn_2L1)^{3+}$ selectively binds with phosphorylated peptides with the addition of a positive charge per phosphate group, $(Zn_2L1)^{3+}$-aided ESI improved the ionization yield of phosphopeptides present in the protein digest,[16] and allowed us to sequence tryptic phosphopeptide by ETD-MS/MS. However, $(Zn_2L1)^{3+}$-aided ETD-MS/MS had one disadvantage: the fragmentation of $(Zn_2L1)^{3+}$ was also induced by ETD and competed with phosphopeptide backbone fragmentation.

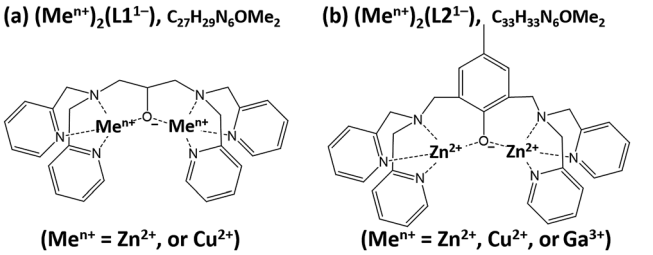

Scheme 1 Structure of the dinuclear complexes (a) $(Me^{n+})_2(L1^{-1})$ and (b) $(Me^{n+})_2(L2^{-1})$, where Me^{n+} is Zn^{2+}, Cu^{2+}, or Ga^{3+}.

Therefore, the development of a new metal complex to replace $(Zn_2L1)^{3+}$ is necessary to suppress the ligand dissociation and to preferentially form the fragments arising from N–Cα bond cleavage.

Similarly to $(Zn_2L1)^{3+}$, dinuclear metal complexes with (2,6-bis[(*N*,*N*′-bis[2-picolyl]amino)methyl]-4-*tert*butylphenol, L2), such as $(Co_2L2)^{3+}$, $(Cu_2L2)^{3+}$, $(Zn_2L2)^{3+}$, $(Ga_2L2)^{5+}$, and $(In_2L2)^{5+}$, have been also tested as phosphate-capture molecules.[35–38] The molecular structure of $(Me^{n+})_2(L2)^{-1}$, where Me^{n+} is Cu^{2+}, Zn^{2+}, or Ga^{3+}, is shown in Scheme 1b. In this study, we tested the applicability of the dimetallic complexes $(Cu_2L1)^{3+}$, $(Cu_2L2)^{3+}$, $(Zn_2L2)^{3+}$, and $(Ga_2L2)^{5+}$ for the ESI-based ETD-MS^2 analysis of phosphopeptides and compared the results with those from the $(Zn_2L1)^{3+}$-aided method. As described above, Zn^{2+} and Ga^{3+} are suitable adductives for peptide sequencing by ETD-MS/MS. In consequence, we used Zn^{2+} and Ga^{3+} as the nuclears in the complex and a complex with Cu^{2+} was used as the reference. First, we evaluated the efficiency for the binding of phosphorylated serine (pS) to the dimetallic complexes from ESI mass spectra. We then used the dimetallic complexes as additives for the ETD-MS/MS analysis of the tryptic phosphopeptides, T18p (NVPLpYK), T19p (HLADLpSK), and T43p (VNQIGpTLSESIK), which have been used as models in previous studies.[16] Although the ESI of these phosphopeptides produced singly and doubly protonated molecules, the triply protonated phosphopeptides were absent. The precise location of the phosphorylation site could not be determined because of the low sequence coverage when doubly protonated molecules were used as the precursors for ETD-MS/MS.[16] In contrast, the use of zinc complexes increased the charge state of phosphopeptides in ESI-MS and facilitated the phosphopeptide sequencing by subsequent ETD-MS/MS analysis. To address the general mechanism for the ETD of the dimetal–ligand–phosphopeptide complexes, the details of the ETD fragmentation pathway were investigated using density functional theory (DFT) calculations.

Experiments

Materials

Synthetic phosphopeptides designed to mimic the fragments produced by the tryptic digestion of yeast enolases, T18p, T19p, and T43p, were purchased from CS Bio Co., Ltd (Shanghai, China). The phosphorylated Nα-acetylated serine–lysine dipeptide

Table 1 Monoisotopic mass (M_m), sequence, and composition of the analyte phosphopeptides used

Analyte	M_m	Sequence	Composition
pS	185.08	pS	$C_3H_8NO_6P$
Ac-pSK	346.11	Ac-pSK	$C_{11}H_{23}N_3O_8P$
T18p	812.39	NVPLpYK	$C_{35}H_{57}O_{12}N_8P$
T19p	862.40	HLADLpSK	$C_{34}H_{59}O_{14}N_{10}P$
T43p	1367.68	VNQIGpTLSESIK	$C_{55}H_{98}O_{23}N_{15}P$

(Ac-pSK) was purchased from GenScript Inc. (NJ, USA). Detailed information on the model phosphopeptides is summarized in Table 1.

Paraformaldehyde, sodium triacetoxyborohydride, 2-pyridinecarboxyaldehyde, 1,3-diamino-2-propanol, copper(II) chloride, zinc(II) chloride, and gallium(III) perchlorate were supplied by Sigma-Aldrich Inc. (MO, USA). Bis(2-pyridylmethyl)amine and *p*-cresol were obtained from Tokyo Chemical Industry Co., Ltd (Tokyo, Japan).

All the solvents used were of high-performance liquid chromatography grade, except for water, which was purified by a Milli-Q® purification system (Millipore; Billerica, MA, USA). The conductivity of the water was 18.2 MΩ cm^{-1}.

Synthesis of ligand molecules

Ligand L1 was synthesized from 1,3-diamino-2-propanol and 2-pyridinecarboxaldehyde by a dehydration condensation in methanol. To facilitate the reaction, sodium triacetoxyborohydride was added. The final concentrations of 1,3-diamino-2-propanol, 2-pyridinecarboxaldehyde, and sodium triacetoxyborohydride were approximately 0.15, 0.75, and 0.84 M, respectively. The reaction was performed for 5 days at room temperature. Ligand L2 was synthesized from *p*-cresol, *p*-formaldehyde, and bis(2-pyridylmethy)amine in ethanol using a literature method.[39] The final concentration of *p*-cresol, *p*-formaldehyde, and bis-(2-pyridylmethy)amine were approximately 0.35, 0.8, and 0.8 M, respectively, and the reaction was performed under reflux conditions over 3 days. The synthesized ligands L1 and L2 were purified by column chromatography with silica gel and recrystallization, respectively.

To obtain dinuclear metal complexes, the synthesized ligands, L1 and L2, were dissolved in methanol at 0.15 M, and the obtained solutions were mixed with aqueous solutions of the corresponding metal salt, *i.e.*, $CuCl_2$, $ZnCl_2$, or $Ga(ClO_4)_3$. The mixing molar ratio of ligand/metal was approximately 1/2. The complexes were obtained by recrystallization.

Measurement of the binding affinity between pS and $(Me^{n+})_2(Lx^{-1})$ by ESI-MS

ESI-MS was used to investigate the trend of binding affinities between pS and $(Me^{n+})_2(Lx^{-1})$, where Me^{n+} is Zn^{2+}, Cu^{2+}, or Ga^{3+}, and L*x* is L1 or L2. The abundances of free $(Me^{n+})_2(Lx^{-1})$ and $(Me^{n+})_2(Lx^{-1})$(pS) complexes were estimated by positive ion ESI-MS using an Orbitrap Exactive mass spectrometer (Thermo Fisher, Bremen, Germany). The dinuclear complexes, $(Me^{n+})_2(Lx^{-1})$, were dissolved in water/methanol (1/1, v/v) at a concentration of 20 μM. The complexation was studied in solutions containing 10 μM $(Me^{n+})_2(Lx^{-1})$(pS) and variable concentrations of pS (from 0.5 to 100 μM). The final concentration of the dinuclear complex was adjusted to 10 μM for all the experiments. The values for the abundance of $(Me^{n+})_2(Lx^{-1})$ and $(Me^{n+})_2(Lx^{-1})$(pS) were estimated from the peak areas of the corresponding signals observed in the ESI mass spectra and the mass balance equation on the total concentration of $(Me^{n+})_2(Lx^{-1})$.

ETD-MS/MS

The analyte peptides were dissolved in water/methanol (1/1, v/v) at a concentration of 10 μM. To produce the dinuclear complex-phosphopeptide by ESI, $(Cu_2Lx)^{3+}$, $(Zn_2Lx)^{3+}$, or $(Ga_2L2)^{5+}$ were added to the peptide solution at concentrations of 100, 40, and 20 μM, respectively. ESI mass spectra were acquired using a 9.4 T Fourier transform ion cyclotron resonance (FT-ICR) mass spectrometer (SolariX FT, Bruker, Germany). The analyte solution was directly infused into the mass spectrometer using ESI. The ion accumulation time, ion cooling time, and time-of-flight values were set to 0.5 s, 20 ms, and 7 ms, respectively. For the ETD-MS/MS experiments, the precursor ions were mass-selected in the quadrupole filter and then reacted with the fluoranthene radical anion. The times for reagent accumulation and the ion/ion reaction were set to 150 and 25 ms, respectively. Total ESI-MS and subsequent ETD-MS/MS mass spectra were obtained by the accumulation of 20 and 100 single mass spectra, respectively.

Computational details

All the electronic structure calculations were performed with Gaussian 16.[40] The geometries for the zinc trihistidine complexes were optimized by DFT calculations using the MN15[41] hybrid functional and double-zeta valence polarized basis sets, *i.e.*, LanL2DZ for the metal atoms and 6-31G(d) for the C, H, O, N, and P atoms. To establish the fragmentation energies, transition state (TS) geometries were also optimized at the MN15/LanL2DZ/6-31G(d) level of theory and confirmed by vibrational frequency analysis to have one imaginary frequency. The relationship between the transition state and the reactants, as well as the intermediates, was checked by intrinsic reaction coordinate analysis[42] starting from the transition state conformation. Single-point energies of the local energy minima and transition state geometries were calculated using the MN15 functional with the 6-31++G(2d,p) basis set. Excited electronic states were calculated using a time-dependent DFT method[43] with the MN15 functional and the 6-31++G(2d,p) basis set.

Notation

In the present study, Zubarev's notation was adopted for the peptide fragment ions.[44] According to this notation, homolytic N–Cα bond cleavage yields the radical $c^\bullet$ and $z^\bullet$ fragments, and the addition of a hydrogen atom to the $c^\bullet$ or $z^\bullet$ fragments produces a c' or z' fragment, respectively. The abstraction of a hydrogen atom from the $c^\bullet$ or $z^\bullet$ fragments produces a c or z fragment, respectively.

Results and discussion

Formation efficiency of the dinuclear metal–pS complexes

First, we focused on the binding properties of dimetallic complexes to pS, which were estimated from the ESI mass spectra. In this study, five dimetallic complexes, $(Zn_2L1)^{3+}$, $(Zn_2L2)^{3+}$, $(Cu_2L1)^{3+}$, $(Cu_2L2)^{3+}$, and $(Ga_2L2)^{5+}$ were tested. Because the utility of the $(Zn_2L1)^{2+}$-aided ETD-MS/MS for phosphopeptide sequencing was described in a previous report,[16] we first discussed the complex formation between $(Zn_2L1)^{3+}$ and pS. Fig. 1a shows the ESI mass spectra of the mixture of $(Zn_2L1)^{3+}$ and pS in different mixing ratios.

As described in the experimental section, $(Zn_2L1)^{3+}$ was synthesized from [L1 + H] and $ZnCl_2$. Thereby, Cl^- would be present as a counter ion of $(Zn_2L1)^{3+}$, and $(Zn_2L1)^{3+}$ was detected as the complex with Cl^-, $[Zn_2L1 + Cl]^{2+}$, when the concentration of pS was lower than that of $(Zn_2L1)^{3+}$ (upper panel of Fig. 1a). In addition, $[ZnL1 + H]^{2+}$ and $[ZnL1 - C_6H_6N]^{2+}$ appeared in the ESI mass spectrum. These ions might be produced by ion-solvent reaction during the ESI process. The proposed structures of $[Zn_2L1 + Cl]^{2+}$ and $[ZnL1 + H]^{2+}$ are described in Scheme 2.

When the concentration of pS increased, the intensity of $[Zn_2L1 + Cl]^{2+}$, $[ZnL1 + H]^{2+}$, and $[ZnL1 - C_6H_6N]^{2+}$ decreased and the intensity of the complex between $(Zn_2L1)^{3+}$ and pS increased (lower panel of Fig. 1a). The complex between $(Zn_2L1)^{3+}$ and pS was detected as the doubly charged form, $[Zn_2L1 + pS - H]^{2+}$. Because $(Zn_2L1)^{3+}$ selectively binds to the phosphate group,[16] positive charges in $[Zn_2L1 + pS - H]^{2+}$ would be located at the $(Zn_2L1)^{3+}$-adducted phosphate group and amino group, which is the most probable site for protonation. The proposed structure of $[Zn_2L1 + pS - H]^{2+}$ are shown in Scheme 2. In addition, $[Zn_2L1 + H_2PO_4]^{2+}$ was observed in the ESI mass spectra and the intensity of $[Zn_2L1 + H_2PO_4]^{2+}$ was increased with increasing the pS concentration. Thus, $[Zn_2L1 + H_2PO_4]^{2+}$ was suggested to originate from the $(Zn_2L1)^{3+}$ and pS complex, as shown in Scheme 2.

Next, we focused on the complexation efficiency of $(Zn_2L1)^{3+}$ binding to pS. To estimate the complexation efficiency, we performed the ESI-MS on a $(Zn_2L1)^{3+}$ and pS mixture at a range of pS concentrations from 0.5 to 40 μM. The concentration of $(Zn_2L1)^{3+}$ was set to 10 μM for all the experiments. Fig. 1b shows the relationship between the signal intensity ratio of

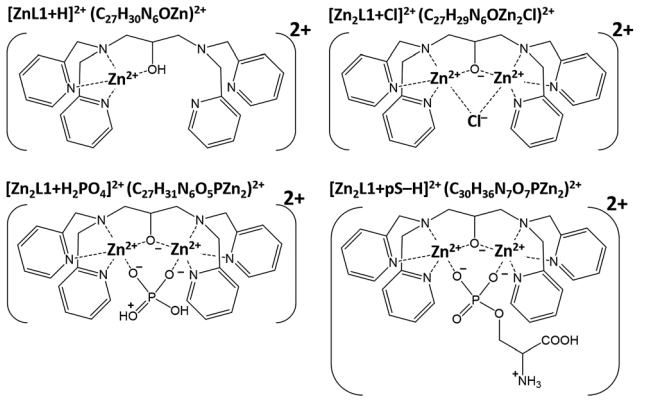

Scheme 2 Proposed structure of ions observed in the ESI mass spectra of $(Zn_2L1)^{3+}$ and pS mixtures, as shown in Fig. 1a.

$(Zn_2L1)^{3+}$ with and without pS, and the total pS concentration between 0.5 and 40 μM. The values of the signal ratio were calculated from the sum of the intensities of all the species assigned in Fig. 1a and undisplayed singly charged species. The yield of the complex between $(Zn_2L1)^{3+}$ and pS increased with the increasing concentration of pS, with 60% of $(Zn_2L_1)^{3+}$ bound to pS when the concentration of $(Zn_2L_1)^{3+}$ and pS were 10 μM.

As in the case of $(Zn_2L1)^{3+}$, $(Zn_2L2)^{3+}$ was selectively bound to the phosphate group of pS, producing $[Zn_2L2 + pS - H]^{2+}$. The relationship between the amount of $(Zn_2L2)^{3+}$ with and without pS at different concentrations of pS is shown in Fig. 1c. The comparison of Fig. 1b and c indicated the yield of complex formation between $(Zn_2L2)^{3+}$ and pS was slightly lower than that of $(Zn_2L1)^{3+}$ and pS. In consequence, $(Zn_2L1)^{3+}$ could capture the phosphate group more efficiently compared with $(Zn_2L2)^{3+}$.

Next, we investigated dinuclear copper complexes, namely $(Cu_2L1)^{3+}$ and $(Cu_2L2)^{3+}$, for their use as phosphate-capture molecules. Fig. 2a shows the ESI mass spectra for the mixture of 10 μM $(Cu_2L1)^{3+}$ and pS with mixing ratios, $[(Cu_2L1)^{3+}]/[pS]$, of 1 and 6. As in the case of $(Zn_2L1)^{3+}$, the ESI mass spectra of the mixture of $(Cu_2L1)^{3+}$ and pS contained chloride and pS adduct forms, $[Cu_2L1 + Cl]^{2+}$ and $[Cu_2L1 + pS - H]^{2+}$. In contrast, the fragment ions $[CuL1 + H]^{2+}$ and $[Cu_2L1 + H_2PO_4]^{2+}$ were absent. In terms of the relative affinities, although $(Zn_2L1)^{3+}$ was mostly bound to pS when 40 μM of pS was added to the $(Zn_2L1)^{3+}$

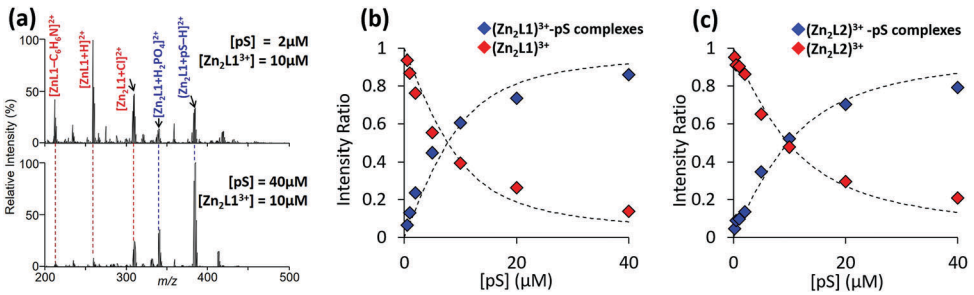

Fig. 1 (a) ESI mass spectra of $(Zn_2L1)^{3+}$ and pS mixtures with different concentration ratios. (b and c) Relationship between the ESI-MS data based on the concentration of pS to the yield of (b) $(Zn_2L1)^{3+}$–pS and (c) $(Zn_2L2)^{3+}$–pS complexes.

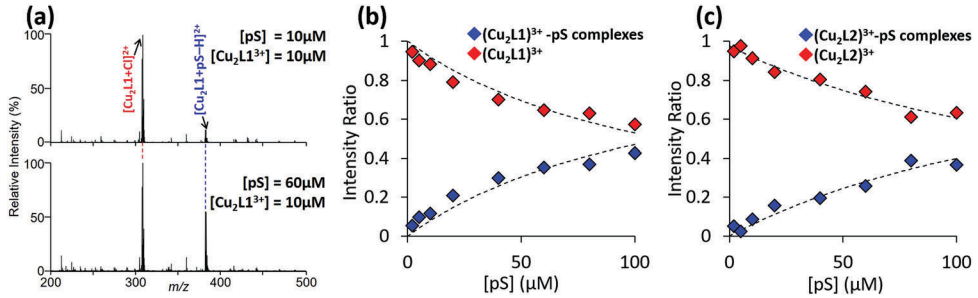

Fig. 2 (a) ESI mass spectra of $(Cu_2L1)^{3+}$ and pS mixtures with different concentration ratios. (b and c) Relationship between the ESI-MS data based on the concentration of pS to the yield of (b) $(Cu_2L1)^{3+}$–pS and (c) $(Cu_2L2)^{3+}$–pS complexes.

solution (Fig. 1a), the chloride adduct of $(Cu_2L1)^{3+}$ was detected as an intense signal at 60 μM of added pS (Fig. 2a). $(Cu_2L2)^{3+}$ showed similar behavior to $(Cu_2L1)^{3+}$ (data not shown). Next, the formation of the $(Cu_2L1)^{3+}$–pS and $(Cu_2L2)^{3+}$–pS complexes were determined using the same procedure as for the $(Zn_2L1)^{3+}$–pS complex (Fig. 2b and c). The comparison of Fig. 1 and 2 indicate that $(Cu_2L1)^{3+}$ and $(Cu_2L2)^{3+}$ have a lower phosphate-capturing ability than $(Zn_2L1)^{3+}$ and $(Zn_2L2)^{3+}$. Thus, the phosphate-capturing ability of a dinuclear metal complex is strongly affected by the type of metal ion.

Next, $(Ga_2L2)^{5+}$ was used as a phosphate-capture molecule. Because Ga is a trivalent metal ion, the use of $(Ga_2L2)^{5+}$ was expected to increase the charge state of the phosphorylated peptides. Fig. 3a shows the ESI mass spectra for the mixture of 10 μM $(Ga_2L2)^{5+}$ and pS with mixing ratios, $[pS]/[(Ga_2L2)^{5+}]$, of 0.2 and 1. When $[pS]/[(Ga_2L2)^{5+}]$ was 0.2, $(Ga_2L2)^{5+}$ was detected as $[Ga_2L2 + O]^{3+}$, $[Ga_2L2 + O + OH]^{2+}$, and $[Ga_2L2 + O + ClO_4]^{2+}$. The source of ClO_4^- was the $Ga(ClO_4)_3$ used for the synthesis of $(Ga_2L2)^{5+}$. According to the previous reports, $(Ga_2L2)^{5+}$ is estimated to be present as $(Ga_2L2)(OH)_2(ClO_4)_3(H_2O)_2$ in the solid state.[38] Because OH^- and ClO_4^- were present as the adduct ions in the ESI mass spectra, the counter ions of $(Ga_2L2)^{5+}$ in solution are suggested as OH^- and ClO_4^-. In consequence, $[Ga_2L2 + O]^{3+}$ might be formed from $[Ga_2L2 + 2OH]^{3+}$ during the ESI process by chemical reaction (1) and so the proposed structure of $[Ga_2L2 + O]^{3+}$ is shown in Scheme 3.

$$[Ga_2L2 + 2OH]^{3+} \rightarrow [Ga_2L2 + O]^{3+} + H_2O \qquad (1)$$

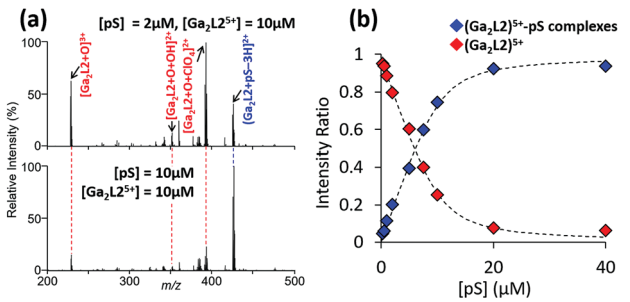

Fig. 3 (a) ESI mass spectra of $(Ga_2L2)^{5+}$ and pS mixtures with different concentration ratios. (b) Relationship between the ESI-MS data based on the concentration of pS to the yield of the $(Ga_2L1)^{5+}$–pS complex.

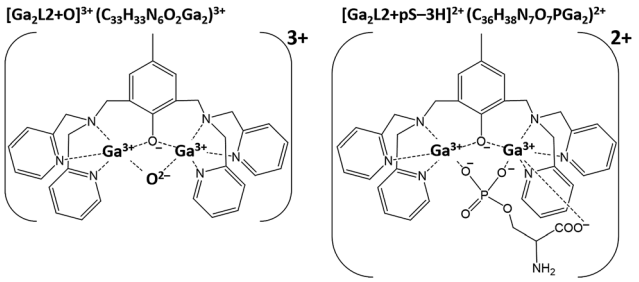

Scheme 3 Structures and formation processes of ions observed in the ESI mass spectra of the $(Ga_2L1)^{5+}$ and pS mixture, as shown in Fig. 2a.

To investigate the reaction behavior of $[Ga_2L2 + 2OH]^{3+}$ in detail, we calculated its optimized geometries by DFT with the MN15/6-31++G(2d,p)//MN15/LanL2DZ/6-31G(d) level (ESI,† Scheme S1). In the lowest energy geometry of $[Ga_2L2 + 2OH]^{3+}$, a hydroxide is strongly coordinated by both Ga^{3+} and another hydroxide is weakly bound to a Ga^{3+}. The proton transfer reaction between hydroxides produced the intermediate complex, IM, consisting of $[Ga_2L2 + O]^{3+}$ and H_2O. The corresponding transition state is TS in Scheme S1 (ESI†), which is 30 kJ mol^{-1} less stable than the reactant. The complete dissociation energy of $[Ga_2L2 + O]^{3+}$ and H_2O from $[Ga_2L2 + 2OH]^{3+}$ was 66 kJ mol^{-1}. Because the internal energies of the ions produced by ESI with the standard parameter sets was estimated to be around 180 kJ mol^{-1},[45] the proposed formation pathway of $[Ga_2L2 + O]^{3+}$ is feasible.

The addition of pS contributes to increasing the signal intensity of the $(Ga_2L2)^{5+}$–pS complex, whereby $[Ga_2L2 + pS - 3H]^{2+}$ (lower panel of Fig. 3a). $(Ga_2L2)^{5+}$ would coordinate to a deprotonated phosphate group and a carboxylic acid group to form $[Ga_2L2 + pS - 3H]^{2+}$. The proposed structure of $[Ga_2L2 + pS - 3H]^{2+}$ is shown in Scheme 3. Fig. 3b shows the relationship between the amount of $(Ga_2L2)^{5+}$ for a total pS concentration in the range of 0.5–40 μM. The amount of $(Ga_2L2)^{3+}$ with and without pS was estimated from the peak areas of $[Ga_2L2 + O]^{3+}$, $[Ga_2L2 + O + OH]^{2+}$, $[Ga_2L2 + O + ClO_4]^{2+}$, and $[Ga_2L2 + pS - 3H]^{2+}$. $(Ga_2L2)^{5+}$ was mostly bound to pS when 20 μM of pS was added to the 10 μM $(Ga_2L2)^{5+}$ solution. A comparison of Fig. 1–3 indicates that $(Ga_2L2)^{5+}$ has the highest binding ability for pS among the complexes tested in this study.

ETD-MS^2 of the dinuclear metal–phosphopeptide complexes

We also investigated the suitability of the complexes for phosphopeptide sequencing by ETD-MS/MS. The phosphopeptide T18p was used as the model peptide with triply charged dinuclear metal–T18p complexes used as the precursor ions for the ETD-MS/MS experiments. Fig. 4 shows the ETD-MS/MS spectra of $[Zn_2L1 + T18p]^{3+}$, $[Zn_2L2 + T18p]^{3+}$, $[Cu_2L1 + T18p]^{3+}$, and $[Ga_2L2 + (T18p - 2H)]^{3+}$. The $(Zn_2L1)^{3+}$ complex was used in our previous work as an additive to increase the charge state of phosphorylated peptides, facilitating phosphopeptide sequencing by ETD-MS/MS.[16] As described in the introduction, the ETD of the $(Zn_2L1)^{3+}$–phosphopeptide complex produced an intense signal for the fragment ion arising from a 92 Da loss, corresponding to ligand degradation. However, the presence of such an intense signal corresponding to the fragment ion because of the 92 Da loss hinders phosphopeptide sequencing. As in previous reports,[16] the ETD of $[Zn_2L1 + (Ac\text{-}pSK - H)]^{2+}$ showed the fragment ion arising from the 92 Da loss as an intense signal, in addition to the formation of fragments due to N–Cα bond cleavage. In contrast, the ETD-MS/MS mass spectrum of $[Zn_2L2 + T18p]^{3+}$ showed a more intense signal corresponding to fragment ions arising from N–Cα bond cleavage, and a lower intensity of the fragment ion arising from the 92 Da loss, as compared to when $(Zn_2L1)^{3+}$ was used.

As shown in Fig. 4c, the ETD of $[Cu_2L1 + T18p]^{3+}$ generated charge-reduced products, $[Cu_2L1 + T18p]^{2+}$, and $[Cu_2L1 + T18p]^{+}$. In addition, $(CuL1)^{+}$ and $[T18p + Cu]^{+}$ were observed as the fragment ions. Importantly, the $[T18p + Cu]^{+}$ contained a monovalent copper atom, indicating that ETD induced the reduction of Cu^{2+}. Because the binding energy between $(Cu_2L1)^{3+}$ and T18p was decreased by the reduction of Cu^{2+} in the complex, $(CuL1)^{+}$ and $[T18p + Cu]^{+}$ would be formed by ETD-MS/MS. This result is in good agreement with the previously reported ETD-MS/MS of Cu^{2+}–peptide complex,[30] where the presence of Cu^{2+} in the precursor ion suppresses N–Cα bond cleavage by ETD-MS/MS.

Regarding Fig. 4d, the ETD of $[Ga_2L2 + (T18p - 2H)]^{3+}$ selectively induced $C_6H_6N^{\bullet}$ losses, leading to $[Ga_2L2 + (T18p - 2H - C_6H_6N)]^{2+}$ and $[Ga_2L2 + (T18p - 2H - 2C_6H_6N)]^{+}$. The $C_6H_6N^{\bullet}$ loss was induced by the electron association to the pyridine ring in the complex, and the N–Cα bond cleavage was completely suppressed by the presence of $(Ga_2L2)^{5+}$ in the precursor.

To investigate of the detailed ETD process of dinuclear metal–T18p complexes, a small peptide, Ac-pSK, was used as the model peptide for the ETD-MS/MS experiments and DFT calculations. The ESI of Ac-pSK and the dinuclear metal complexes mixture produced doubly charged complexes, which were used as the precursor ions for the ETD-MS/MS experiments. Fig. 5 shows the ETD-MS/MS spectra of $[Zn_2L1 + (Ac\text{-}pSK - H)]^{2+}$, $[Zn_2L2 + (Ac\text{-}pSK - H)]^{2+}$, $[Cu_2L1 + (Ac\text{-}pSK - H)]^{2+}$, and $[Ga_2L2 + (Ac\text{-}pSK - 3H)]^{2+}$. First, we focused on the ETD-MS/MS spectra of $[Zn_2L1 + (Ac\text{-}pSK - H)]^{2+}$ and $[Zn_2L2 + (Ac\text{-}pSK - H)]^{2+}$.

For comparison of the $(Zn_2L1)^{3+}$- and $(Zn_2L2)^{3+}$-aided methods, the ETD mass spectra of $[Zn_2L1 + (Ac\text{-}pSK - H)]^{2+}$

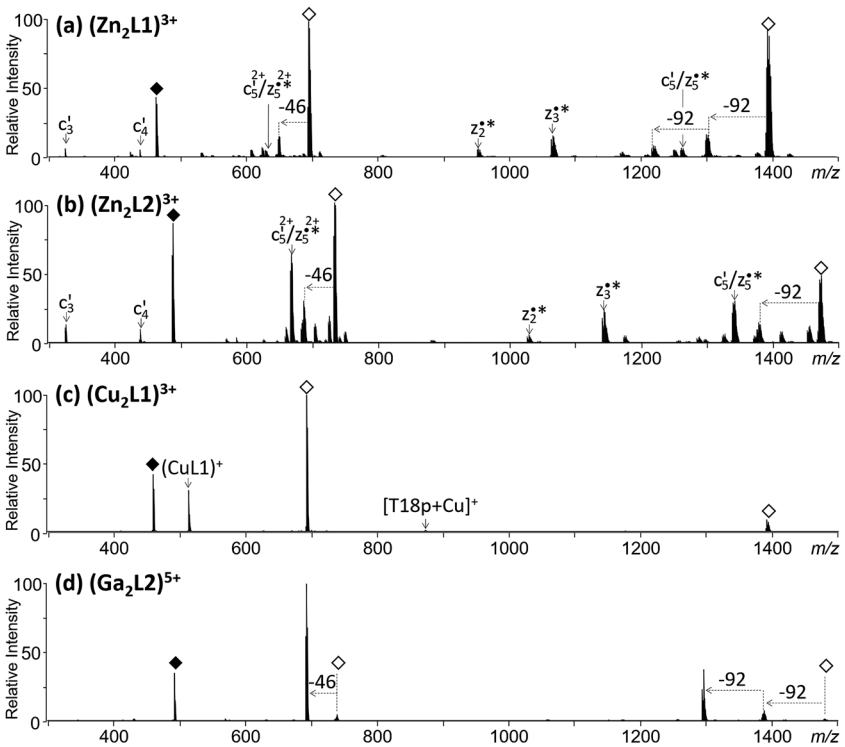

Fig. 4 ETD-MS/MS mass spectra of the doubly charged complexes: (a) $[Zn_2L1 + T18p]^{3+}$, (b) $[Zn_2L2 + T18p]^{3+}$, (c) $[Cu_2L1 + T18p]^{3+}$, and (d) $[Ga_2L2 + (T18p - 2H)]^{3+}$. Asterisks and black squares indicate the precursor ions and charge-reduced products, respectively. "−92" is the unwanted ligand degradation.

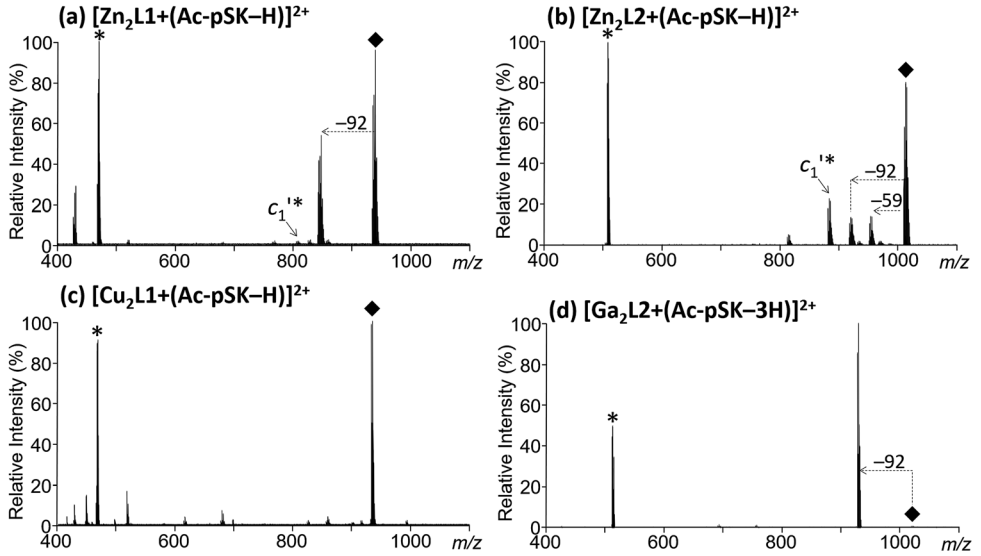

Fig. 5 ETD-MS/MS mass spectra of the doubly charged complexes: (a) $[Zn_2L1 + (Ac\text{-}pSK - H)]^{2+}$, (b) $[Zn_2L2 + (Ac\text{-}pSK - H)]^{2+}$, (c) $[Cu_2L1 + (Ac\text{-}pSK - H)]^{2+}$, and (d) $[Ga_2L2 + (Ac\text{-}pSK - 3H)]^{2+}$. Asterisks and black squares indicate the precursor ions and charge-reduced products, respectively. "−92" is the unwanted ligand degradation, whereas "c_1'" and "−59" are the desired N–Cα fragmentation.

and $[Zn_2L2 + (Ac\text{-}pSK - H)]^{2+}$ showed both fragments due to the 92 Da loss and N–Cα bond cleavage, whereas the yields were different from $[Zn_2L1 + (Ac\text{-}pSK - H)]^{2+}$ and $[Zn_2L2 + (Ac\text{-}pSK - H)]^{2+}$, as in the case of $[Zn_2L1 + T18]^{3+}$ and $[Zn_2L2 + T18]^{3+}$. The potential fragmentation pathways induced by ETD are summarized in Scheme 4. Although the loss of acetyl groups through an intermediate, R3, was expected to occur during the ETD process of $[Zn_2L1 + (Ac\text{-}pSK - H)]^{2+}$, the corresponding signal for $[Zn_2L1 + (Ac\text{-}pSK - H) - 59]^{+\bullet}$ was absent, as can be seen in Fig. 5a, indicating that N–Cα bond cleavage is a low-efficiency process.

The ETD-MS/MS mass spectrum of $[Zn_2L2 + (Ac\text{-}pSK - H)]^{2+}$ showed a more intense signal corresponding to fragment ions arising from N–Cα bond cleavage (c_1'), and a lower intensity of the fragment ion arising from the 92 Da loss, as compared to when $(Zn_2L1)^{3+}$ was used. To explain these differences, the ETD processes of $[Zn_2L1 + (Ac\text{-}pSK - H)]^{2+}$ and $[Zn_2L2 + (Ac\text{-}pSK - H)]^{2+}$ were investigated by DFT. Regarding the initial ETD step, electron association occurs either at the pyridine ring in the ligand, the protonated amino group, or the π* antibonding orbital of the peptide bond. The electron association to the pyridine ring in the doubly charged complex and the subsequent geometry relaxation generated the zwitterionic radical R1 (as shown in Scheme 4), whereas R2 and R3 were generated by electron association to the π* antibonding orbital of the peptide bond and protonated amino group, respectively. The detailed reaction energies, including the transition state barrier (TS) and intermediate (IM) for the ETD fragmentation of $[Zn_2L1 + (Ac\text{-}pSK - H)]^{2+}$ and $[Zn_2L2 + (Ac\text{-}pSK - H)]^{2+}$, are summarized in Table 2 and the corresponding geometries are shown in the ESI,† Scheme S2. Although $[Zn_2L1 + (Ac\text{-}pSK - H) - 92]^{+}$ is the most intense fragment ion in Fig. 5a, the transition state barrier for $C_6H_6N^{\bullet}$ loss from R1 was 121 kJ mol^{-1}, which is higher than that for the N–Cα bond cleavage of R2 and R3. Additionally, the change from

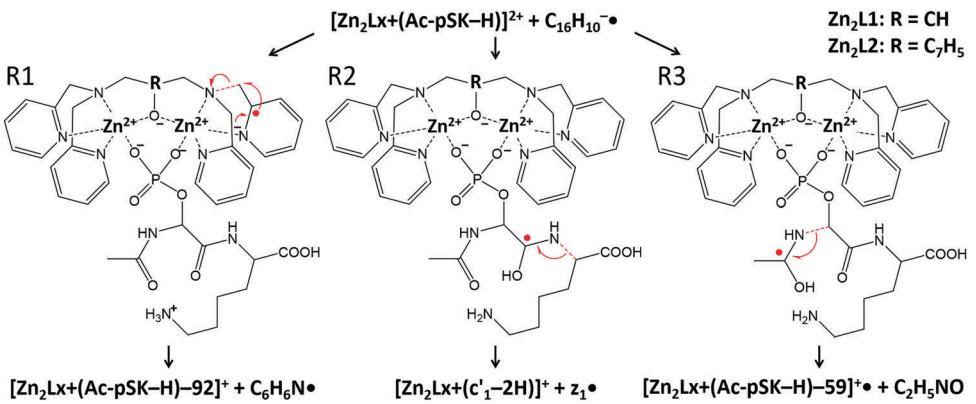

Scheme 4 ETD mechanism of $[Zn_2L1 + (Ac\text{-}pSK - H)]^{2+}$ and $[Zn_2L2 + (Ac\text{-}pSK - H)]^{2+}$. Detailed information, including the transition state geometries for fragmentation, is shown in the ESI,† Scheme S2.

Table 2 Reaction energies of ETD-induced fragmentation, as shown in Scheme 4. The relative energies (kJ mol^{-1}) were obtained from MN15/6-31++G(2d,p)//MN15/LanL2DZ/6-31G(d) calculations

Reaction	TS	IM	Products
R1 → $[Zn_2L1 + (Ac\text{-}pSK - H) - 92]^+ + C_6H_6N^\bullet$	121	116	213
R1′ → $[Zn_2L2 + (Ac\text{-}pSK - H) - 92]^+ + C_6H_6N^\bullet$	77	27	156
R2 → $[Zn_2L1 + (c_1' - 2H)]^+ + z_1^\bullet$	20	−42	139
R2′ → $[Zn_2L2 + (c_1' - 2H)]^+ + z_1^\bullet$	30	−67	143
R3 → $[Zn_2L1 + (Ac\text{-}pSK - H) - 59]^{+\bullet} + C_2H_5NO$	41	−33	27
R3′ → $[Zn_2L2 + (Ac\text{-}pSK - H) - 59]^{+\bullet} + C_2H_5NO$	42	−35	24

$(Zn_2L1)^{3+}$ to $(Zn_2L2)^{3+}$ significantly suppressed the formation of the fragment arising from a 92 Da loss, whereas R1′ had a lower transition state barrier for $C_6H_6N^\bullet$ loss than R1. The DFT calculations revealed that the yield of the fragment ion does not depend on the transition state energy for fragmentation. The fragments arising from N–Cα bond cleavage and $C_6H_6N^\bullet$ loss originated from different electronic states of the charge-reduced complexes. In other words, the intermediate radicals, R1, R2, and R3, were formed by these different processes. Therefore, the yields of $[Zn_2L1 + (Ac\text{-}pSK - H) - 92]^+$, $[Zn_2L1 + (c_1' - 2H)]^+$, and $[Zn_2L1 + (Ac\text{-}pSK - H) - 59]^{+\bullet}$ could be expected to reflect the amounts of R1, R2, and R3, respectively.

To investigate the intermediate radicals formed (R1, R2, and R3), we focused on the initial step of ETD, *i.e.*, the electron-attachment process of doubly charged complexes, which we modeled using time-dependent (TD) DFT calculations. Fig. 6a and b show the molecular orbitals for the ground state and excited states of $[Zn_2L1 + (Ac\text{-}pSK - H)]^{+\bullet}$ and $[Zn_2L2 + (Ac\text{-}pSK - H)]^{+\bullet}$, respectively, and their corresponding vertical excitation energies. Although the electron-transfer process does not occur in a monochromatic way, the calculated vertical excitation energies would relate to the relative energies for the excited state of the $[Zn_2L1 + (Ac\text{-}pSK - H)]^{+\bullet}$ and $[Zn_2L2 + (Ac\text{-}pSK - H)]^{+\bullet}$, which were formed by ETD. The ground state and excited states, R1a–R1e in Fig. 6a and R1a′–R1e′ in Fig. 6b, lead to the zwitterionic radical R1 in Scheme 4, which has a pyridine radical anion. The intermediate radicals R1 and R1′ then underwent $C_6H_6N^\bullet$ loss, forming $[Zn_2L1 + (Ac\text{-}pSK - H) - 92]^{+\bullet}$ and $[Zn_2L2 + (Ac\text{-}pSK - H) - 92]^{+\bullet}$, respectively. In contrast, $[Zn_2L1 + (c_1' - 2H)]^+$ and $[Zn_2L1 + (Ac\text{-}pSK - H) - 59]^{+\bullet}$ would be formed from the excited state configurations R2/R2′ and R3/R3′ in Fig. 6, respectively. The electron attachment to excited states R2/R2′ and R3/R3′ produced an aminoketyl anion radical and ammonium radical, respectively. Subsequently, these radicals were involved in intermolecular hydrogen transfer to give aminoketyl radical intermediates, R2/R2′ and R3/R3′ in Scheme 4. The aminoketyl radical intermediates immediately underwent N–Cα bond cleavage, as shown in Scheme 4. By comparing Fig. 5a and b, the relative energies of the excited states R2′ and R3′ in $[Zn_2L2 + (Ac\text{-}pSK - H)]^{+\bullet}$ can be seen to be lower than R2 and R3 in $[Zn_2L1 + (Ac\text{-}pSK - H)]^{+\bullet}$. Therefore, the $[Zn_2L2 + (Ac\text{-}pSK - H)]^{2+\bullet}$ complex can produce aminoketyl radical intermediates R1′ and R2′ more efficiently than $[Zn_2L1 + (Ac\text{-}pSK - H)]^{2+\bullet}$.

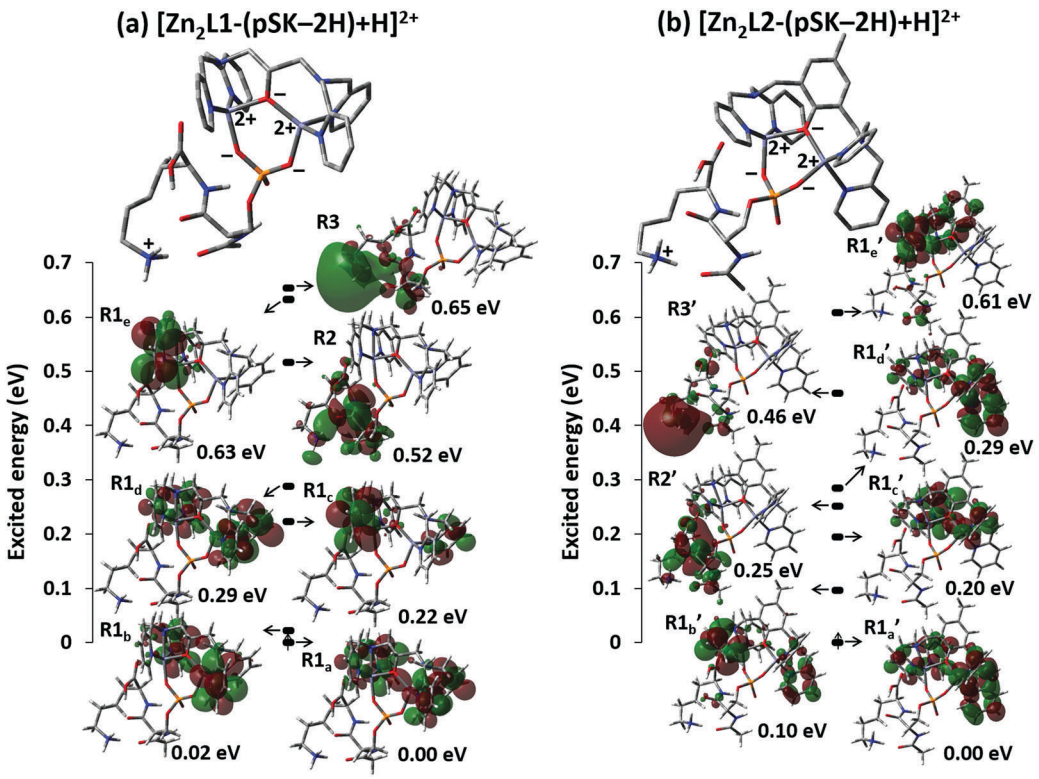

Fig. 6 Optimized conformations and electronic state diagrams for vertical electron attachment of the doubly charged complexes (a) $[Zn_2L1 + Ac\text{-}pSK - H]^{2+}$ and (b) $[Zn_2L2 + Ac\text{-}pSK - H]^{2+}$. The optimized conformations were obtained at the MN15/LanL2DZ/6-31G(d) level of theory, and the excitation energies (eV) were obtained from TD-MN15/6-31++G(2d,p) calculations.

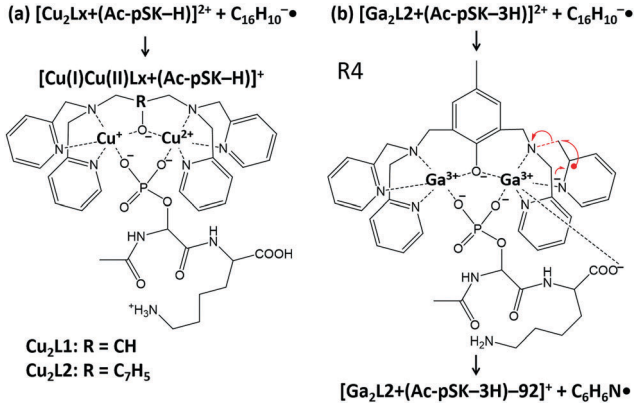

Scheme 5 ETD mechanisms of (a) $[Cu_2L1 + (Ac\text{-}pSK - H) + H]^{2+}$ and (b) $[Ga_2L2 + (Ac\text{-}pSK - 3H)]^{2+}$. Detailed information, including the transition state geometry for the fragmentation of R4, is shown in the ESI,† Scheme S3.

In contrast with the complexes of $(Zn_2L1)^{3+}$ and $(Zn_2L2)^{3+}$, the ETD of $[Cu_2L1 + (Ac\text{-}pSK - H)]^{2+}$ generated products involving charge reduction, as in the case of $[Cu_2L1 + T18p]^{3+}$. The ETD of $[Cu_2L2 + (Ac\text{-}pSK - H)]^{2+}$ showed a similar result (data not shown). As expected from the experimental results, the DFT calculations indicated that the electron association of $[Cu_2L1 + (Ac\text{-}pSK - H)]^{2+}$ and $[Cu_2L2 + (Ac\text{-}pSK - H)]^{2+}$ produced charge-reduced complexes containing a monovalent copper cation, Cu^+ (Scheme 5a), while the formation of amino-ketyl radicals is largely suppressed by the presence of Cu^{2+} in the precursor.

Fig. 5d shows the ETD-MS/MS mass spectrum of $[Ga_2L2 + (Ac\text{-}pSK - 3H)]^{2+}$, which selectively produced its fragment ion by $C_6H_6N^\bullet$ loss. DFT calculations indicated that an electron selectively associates with the pyridine ring in the ligand and the subsequent geometry relaxation generates the zwitterionic radical R4 (Scheme 5b). Then, R4 undergoes fragmentation by $C_6H_6N^\bullet$ loss. According to the MN15/6-31++G(2d,p)//MN15/LanL2DZ/6-31G(d) level of calculation, the transition state energy barrier for $C_6H_6N^\bullet$ loss was 71 kJ mol^{-1}, and the bond cleavage results in the formation of the IM, which was 19 kJ mol^{-1} more stable than R4. Subsequently, the complete dissociation energy of $[Ga_2L2 + (Ac\text{-}pSK - 3H) - 92]^+$ and $C_6H_6N^\bullet$ was 127 kJ mol^{-1} above that of R4. The geometries of the transition state barrier (TS) and intermediate (IM) for the corresponding fragmentation are shown in the ESI,† Scheme S3. In summary, the use of $(Ga_2L2)^{5+}$ for ETD-MS/MS preferentially provided for 92 Da loss and did not induce peptide backbone fragmentation. Therefore, $(Ga_2L2)^{5+}$-aided ETD was not suitable for phosphopeptide sequencing, although $(Ga_2L2)^{5+}$ strongly binds to the phosphate group.

Utility of $(Zn_2L2)^{3+}$ for phosphopeptide sequencing by ETD-MS/MS

As described in the previous section, the use of $(Zn_2L2)^{3+}$ potentially facilitates phosphopeptide sequencing by ETD-MS/MS. Next, we used, T19p and T43p as tryptic phosphopeptide models. These phosphopeptides have been used as models in previous studies, but the precise location of the phosphorylation site could not be determined because of the low sequence coverage when doubly protonated molecules were used as the precursors for ETD-MS/MS.[16] Fig. 7 shows the $(Zn_2L2)^{3+}$-aided ETD-MS/MS mass spectra when triply charged $(Zn_2L2)^{3+}$–phosphopeptide complexes were used as the precursors. $(Zn_2L2)^{3+}$-aided ETD-MS/MS provided almost full sequence coverage, including information concerning the phosphorylation site. For comparison with the previously reported $(Zn_2L1)^{3+}$-aided ETD-MS/MS method, the change from $(Zn_2L2)^{3+}$ to $(Zn_2L1)^{3+}$ significantly suppressed the yield of the fragment arising from the 92 Da loss. In addition, the efficiency of N–Cα bond cleavage was improved, indicating that $(Zn_2L2)^{3+}$-aided ETD-MS/MS is a useful method for the sequencing of phosphopeptides.

Conclusion

The dinuclear metal complexes $(Zn_2L1)^{3+}$, $(Zn_2L2)^{3+}$, $(Cu_2L1)^{3+}$, $(Cu_2L2)^{3+}$, and $(Ga_2L2)^{5+}$ were investigated for use as additives for the analysis of phosphopeptides by ESI-based ETD-MS/MS. Although all the dinuclear metal complexes could selectively bound to phosphate compounds, their affinity was dependent on the type of metal present in the complex. The order of

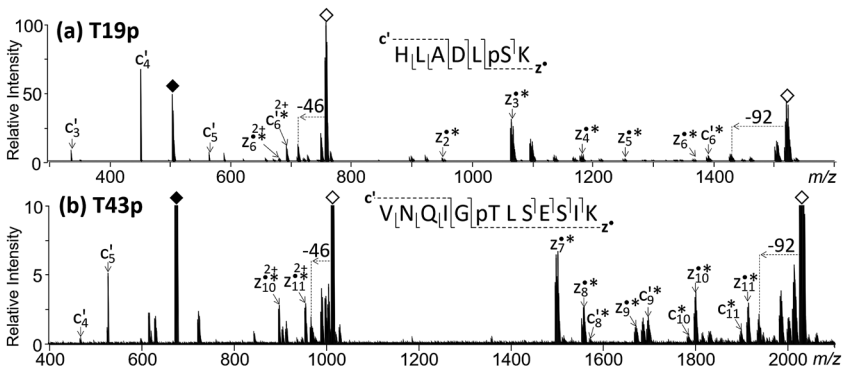

Fig. 7 ETD-MS/MS mass spectra of triply charged $(Zn_2L2)^{3+}$–phosphopeptide complexes. The c' and $z^\bullet$ fragments annotated with asterisks (c'^* and $z^{\bullet *}$) correspond to the $(Zn_2L2)^{3+}$ adduct on the c' and $z^\bullet$ fragments. Black and white squares indicate the precursor ions and charge-reduced products, respectively.

binding affinity for pS was $(Ga_2L2)^{5+} > (Zn_2L1)^{3+} \gtrsim (Zn_2L2)^{3+} > (Cu_2L1)^{3+} > (Cu_2L2)^{3+}$.

The type of metal ion in the complex also strongly influenced the ETD fragmentation. Regarding the ETD of the complexes with copper, Cu^{2+} acted as an electron trap, and peptide fragmentation was largely suppressed. In contrast, $(Ga_2L2)^{5+}$ strongly bound to pS and phosphopeptides, whereas the ETD of the $(Ga_2L2)^{5+}$–phosphopeptide complex mainly led to $C_6H_6N^{\bullet}$ loss. Therefore, $(Cu_2L1)^{3+}$, $(Cu_2L2)^{3+}$, and $(Ga_2L2)^{5+}$-aided ETD-MS/MS could not be used for phosphopeptide sequencing.

The zinc dinuclear complexes, $(Zn_2L1)^{3+}$ and $(Zn_2L2)^{3+}$, efficiently bound to the phosphorylated compounds. In particular, the use of $(Zn_2L2)^{3+}$ facilitated N–Cα bond cleavage by ETD-MS/MS compared with the $(Zn_2L1)^{3+}$-aided method. The yield of the fragments arising from N–Cα bond cleavage reflected the number of aminoketyl radical intermediates, as predicted by TD-DFT calculations. The computational results indicated that the $(Zn_2L2)^{3+}$–phosphopeptide complex could efficiently produce aminoketyl radical intermediates by ETD, facilitating phosphopeptide sequencing. To apply $(Zn_2L2)^{3+}$-aided ETD for large-scale phosphopeptide analysis, the method should be combined with a liquid chromatography mass spectrometry (LC-MS) system. Although the $(Zn_2L2)^{3+}$–phosphopeptide complex would not be stable during the chromatographic separation process, the post-column addition of $(Zn_2L2)^{3+}$ can produce the complex. The further investigation for $(Zn_2L2)^{3+}$-aided ETD combined with LCMS would promote the wider application of this method.

Conflicts of interest

There are no conflicts to declare.

Acknowledgements

DA acknowledge Issey Osaka, for allowing to use FT-ICR MS instrument. This work was supported by JSPS KAKENHI grant number 17K14508. The computations of molecular structures in this work were supported by Research Center for Computational Science, Okazaki and Center for Computational Sciences. The experiments were partly supported by Nanotechnology Platform Program of the Ministry of Education, Culture, Sports, Science and Technology (MEXT), Japan, and the Plateforme de Biophysico-Chimie Structurale of the IECB, France.

References

1 P. Cohen, The Regulation of Protein Function by Multisite Phosphorylation-A 25 Year Update, *Trends Biochem. Sci.*, 2000, **25**, 596–601.
2 T. Hunter, Signaling-2000 and Beyond, *Cell*, 2000, **100**, 113–127.
3 P. J. Boersema, S. Mohammed and A. J. Heck, Phosphopeptide Fragmentation and Analysis by Mass Spectrometry, *J. Mass Spectrom.*, 2009, **44**, 861–878.
4 A. M. Palumbo, S. A. Smith, C. L. Kalcic, M. Dantus, P. M. Stemmer and G. E. Reid, Tandem Mass Spectrometry Strategies for Phosphoproteome Analysis, *Mass Spectrom. Rev.*, 2011, **30**, 600–625.
5 D. Asakawa and M. Takayama, Mass Spectrometric Characterization of Phosphorylated Peptides using MALDI In-Source Decay *via* Redox Reactions, *J. Mass Spectrom.*, 2012, **47**, 180–187.
6 D. Asakawa, H. Takahashi, S. Iwamoto and K. Tanaka, De Novo Sequencing of Tryptic Phosphopeptides using Matrix-Assisted Laser Desorption/Ionization Based Tandem Mass Spectrometry with Hydrogen Atom Attachment, *Anal. Chem.*, 2018, **90**, 2701–2707.
7 R. A. Zubarev, N. L. Kelleher and F. W. McLafferty, Electron Capture Dissociation of Multiply Charged Protein Cations. A Nonergodic Process, *J. Am. Chem. Soc.*, 1998, **120**, 3265–3266.
8 J. E. Syka, J. J. Coon, M. J. Schroeder, J. Shabanowitz and D. F. Hunt, Peptide and Protein Sequence Analysis by Electron Transfer Dissociation Mass Spectrometry, *Proc. Natl. Acad. Sci. U. S. A.*, 2004, **101**, 9528–9533.
9 N. L. Kelleher, Peer Reviewed: Top-Down Proteomics, *Anal. Chem.*, 2004, **76**, 196A–203A.
10 J. J. Coon, Collisions or Electrons? Protein Sequence Analysis in the 21st Century, *Anal. Chem.*, 2009, **81**, 3208–3215.
11 H. Zhou, Z. Ning, A. E. Starr, M. Abu-Farha and D. Figeys, Advancements in Top-down Proteomics, *Anal. Chem.*, 2012, **84**, 720–734.
12 R. A. Zubarev, D. M. Horn, E. K. Fridriksson, N. L. Kelleher, N. A. Kruger, M. A. Lewis, B. K. Carpenter and F. W. McLafferty, Electron Capture Dissociation for Structural Characterization of Multiply Charged Protein Cations, *Anal. Chem.*, 2000, **72**, 563–573.
13 M. Sobczyk, I. Anusiewicz, J. Berdys-Kochanska, A. Sawicka, P. Skurski and J. Simons, Coulomb-Assisted Dissociative Electron Attachment: Application to a Model Peptide, *J. Phys. Chem. A*, 2005, **109**, 250–258.
14 E. A. Syrstad and F. Tureček, Toward a General Mechanism of Electron Capture Dissociation, *J. Am. Soc. Mass Spectrom*, 2005, **16**, 208–224.
15 D. Asakawa, A. Yamashita, S. Kawai, T. Takeuchi and Y. Wada, N–Cα Bond Cleavage of Zinc–Polyhistidine Complexes in Electron Transfer Dissociation Mediated by Zwitterion Formation: Experimental Evidence and Theoretical Analysis of the Utah-Washington Model, *J. Phys. Chem. B*, 2016, **120**, 891–901.
16 D. Asakawa and I. Osaka, High-Confidence Sequencing of Phosphopeptides by Electron Transfer Dissociation Mass Spectrometry Using Dinuclear Zinc(II) Complex, *Anal. Chem.*, 2016, **88**, 12393–12402.
17 M. Rožman and S. J. Gaskell, Charge State Dependent Top-Down Characterisation Using Electron Transfer Dissociation, *Rapid Commun. Mass Spectrom.*, 2012, **26**, 282–286.
18 D. M. Good, M. Wirtala, G. C. McAlister and J. J. Coon, Performance Characteristics of Electron Transfer Dissociation Mass Spectrometry, *Mol. Cell. Proteomics*, 2007, **6**, 1942–1951.

19 C. K. Frese, A. F. Altelaar, M. L. Hennrich, D. Nolting, M. Zeller, J. Griep-Raming, A. J. Heck and S. Mohammed, Improved Peptide Identification by Targeted Fragmentation Using CID, HCD and ETD on an LTQ-Orbitrap Velos, *J. Proteome Res.*, 2011, **10**, 2377–2388.
20 T. G. Flick, W. A. Donald and E. R. Williams, Electron Capture Dissociation of Trivalent Metal Ion-Peptide Complexes, *J. Am. Soc. Mass Spectrom*, 2013, **24**, 193–201.
21 D. Asakawa, T. Takeuchi, A. Yamashita and Y. Wada, Influence of Metal–Peptide Complexation on Fragmentation and Inter-Fragment Hydrogen Migration in Electron Transfer Dissociation, *J. Am. Soc. Mass Spectrom*, 2014, **25**, 1029–1039.
22 D. Asakawa and Y. Wada, Electron Transfer Dissociation Mass Spectrometry of Peptides Containing Free Cysteine Using Group XII Metals as a Charge Carrier, *J. Phys. Chem. B*, 2014, **118**, 12318–12325.
23 X. Chen, G. Liu, Y. L. Elaine Wong, L. Deng, Z. Wang, W. Li and T. W. Dominic Chan, Dissociation of trivalent metal ion (Al(3) (+), Ga(3) (+), In(3) (+) and Rh(3) (+))-peptide complexes under electron capture dissociation conditions, *Rapid Commun. Mass Spectrom.*, 2016, **30**, 705–710.
24 J. J. Commodore and C. J. Cassady, Effects of Acidic Peptide Size and Sequence on Trivalent Praseodymium Adduction and Electron Transfer Dissociation Mass Spectrometry, *J. Mass Spectrom.*, 2017, **52**, 218–229.
25 A. T. Iavarone, K. Paech and E. R. Williams, Effects of Charge State and Cationizing Agent on the Electron Capture Dissociation of a Peptide, *Anal. Chem.*, 2004, **76**, 2231–2238.
26 Y. M. Fung, H. Liu and T. W. Chan, Electron Capture Dissociation of Peptides Metalated with Alkaline-Earth Metal Ions, *J. Am. Soc. Mass Spectrom*, 2006, **17**, 757–771.
27 X. Chen, Y. M. Fung, W. Y. Chan, P. S. Wong, H. S. Yeung and T. W. Chan, Transition Metal Ions: Charge Carriers that Mediate the Electron Capture Dissociation Pathways of Peptides, *J. Am. Soc. Mass Spectrom.*, 2011, **22**, 2232–2245.
28 B. Bogdanov, X. Zhao, D. B. Robinson and J. Ren, Electron Capture Dissociation Studies of the Fragmentation Patterns of Doubly Protonated and Mixed Protonated-Sodiated Peptoids, *J. Am. Soc. Mass Spectrom*, 2014, **25**, 1202–1216.
29 J. J. Commodore and C. J. Cassady, The Effects of Trivalent Lanthanide Cationization on the Electron Transfer Dissociation of Acidic Fibrinopeptide B and its Analogs, *J. Am. Soc. Mass Spectrom*, 2016, **27**, 1499–1509.
30 D. Asakawa and E. De Pauw, Difference of Electron Capture and Transfer Dissociation Mass Spectrometry on Ni^{2+}-, Cu^{2+}- and Zn^{2+}-Polyhistidine Complexes in the Absence of Remote Protons, *J. Am. Soc. Mass Spectrom*, 2016, **27**, 1165–1175.
31 X. Chen, W. Y. Chan, P. S. Wong, H. S. Yeung and T. W. Chan, Formation of Peptide Radical Cations ($M^{+\bullet}$) in Electron Capture Dissociation of Peptides Adducted with Group IIB Metal Ions, *J. Am. Soc. Mass Spectrom*, 2011, **22**, 233–244.
32 E. Kinoshita, M. Takahashi, H. Takeda, M. Shiro and T. Koike, Recognition of Phosphate Monoester Dianion by An Alkoxide-Bridged Dinuclear Zinc(II) Complex, *Dalton Trans.*, 2004, 1189–1193.
33 E. Kinoshita, A. Yamada, H. Takeda, E. Kinoshita-Kikuta and T. Koike, Novel Immobilized Zinc(II) Affinity Chromatography for Phosphopeptides and Phosphorylated Proteins, *J. Sep. Sci.*, 2005, **28**, 155–162.
34 E. Kinoshita, E. Kinoshita-Kikuta, K. Takiyama and T. Koike, Phosphate-Binding Tag, A New Tool to Visualize Phosphorylated Proteins, *Mol. Cell. Proteomics*, 2006, **5**, 749–757.
35 S. Svane, F. Kryuchkov, A. Lennartson, C. J. McKenzie and F. Kjeldsen, Overcoming the Instability of Gaseous Peptide Phosphate Ester Groups by Dimetal Protection, *Angew. Chem.*, 2012, **51**, 3216–3219.
36 S. Svane, V. Gorshkov and F. Kjeldsen, Charge Inversion of Phospholipids by Dimetal Complexes for Positive Ion-Mode Electrospray Ionization Mass Spectrometry Analysis, *Anal. Chem.*, 2015, **87**, 8732–8739.
37 S. Svane, T. J. Jorgensen, C. J. McKenzie and F. Kjeldsen, Effect of Metals in Biomimetic Dimetal Complexes on Affinity and Gas-Phase Protection of Phosphate Esters, *Anal. Chem.*, 2015, **87**, 7060–7068.
38 S. Svane, F. Kjeldsen, V. McKee and C. J. McKenzie, The Selectivity of Water-Based Pyrophosphate Recognition is Tuned by Metal Substitution in Dimetallic Receptors, *Dalton Trans.*, 2015, **44**, 11877–11886.
39 M. Ghiladi, C. J. McKenzie, A. Meier, A. K. Powell, J. Ulstrup and S. Wocadlo, Dinuclear Iron(III)-Metal(II) Complexes as Structural Core Models for Purple Acid Phosphatases, *J. Chem. Soc., Dalton Trans.*, 1997, 4011–4018.
40 M. J. Frisch, G. W. Trucks, H. B. Schlegel, G. E. Scuseria, M. A. Robb, J. R. Cheeseman, G. Scalmani, V. Barone, *et al.*, *Gaussian 16; Revision A.03*, Gaussian, Inc., Wallingford CT, 2016.
41 H. S. Yu, X. He, S. L. Lia and D. G. Truhlar, MN15: A Kohn-Sham Global-Hybrid Exchange-Correlation Density Functional with Broad Accuracy for Multi-Reference and Single-Reference Systems and Noncovalent Interactions, *Chem. Sci.*, 2016, **7**, 5032–5051.
42 K. Fukui, The Path of Chemical Reactions-the IRC Approach, *Acc. Chem. Res.*, 1981, **14**, 363–368.
43 R. E. Stratmann, G. E. Scuseria and M. J. Frisch, An Efficient Implementation of Time-Dependent Density-Functional Theory for the Calculation of Excitation Energies of Large Molecules, *J. Chem. Phys.*, 1998, **109**, 8218–8224.
44 R. A. Zubarev, Reactions of Polypeptide Ions with Electrons in the Gas Phase, *Mass Spectrom. Rev.*, 2003, **22**, 57–77.
45 V. Gabelica and E. De Pauw, Internal energy and fragmentation of ions produced in electrospray sources, *Mass Spectrom. Rev.*, 2005, **24**, 566–587.